



Article

A Framework Based on LIDs and Storage Pumping Stations for Urban Waterlogging

Huayue Li ^{1,2}, Qinghua Luan ^{1,*}, Jiahong Liu ³ , Cheng Gao ² and Hong Zhou ²

¹ National Cooperative Innovation Center for Water Safety & Hydro Science, Hohai University, Nanjing 210024, China; 211601010108@hhu.edu.cn

² College of Hydrology and Water Resources, Hohai University, Nanjing 210098, China; cgao@hhu.edu.cn (C.G.); hong_zhou@hhu.edu.cn (H.Z.)

³ Key Laboratory of River Basin Digital Twinning of Ministry of Water Resources, Beijing 100038, China; liujh@iwhr.com

* Correspondence: 20200050@hhu.edu.cn

Abstract: Climate change has resulted in an increase in extreme rainstorm events, posing the challenges of urban waterlogging and runoff pollution. Low Impact Development (LID) is widely used to address the issues above, but its effectiveness is unknown in mountainous areas. Due to a flash flood and high flood peak, storage pumping stations are also needed to drain. Thus, a framework composed of storage pumping stations and Low Impact Developments (LIDs) was proposed based on the topography and the regional upstream and downstream relationships. The water quantity in this framework is applied to YI County in Hebei Province, China. The results showed that individual LIDs effectively reduced runoff volume, with the implementation area being more crucial than the location. Combining storage pumping stations with LIDs significantly reduces peak outflow and delays it by 5 to 51 min. The combined downstream implementation of storage pumping stations and LIDs yielded the most effective results. These findings offer important insights and management strategies for controlling waterlogging in mountainous cities of developing countries.

Keywords: LIDs; RS; scheme optimization; storage pumping station; SWMM; upstream and downstream relationships; urban waterlogging



Citation: Li, H.; Luan, Q.; Liu, J.; Gao, C.; Zhou, H. A Framework Based on LIDs and Storage Pumping Stations for Urban Waterlogging. *Remote Sens.* **2024**, *16*, 1207. <https://doi.org/10.3390/rs16071207>

Academic Editor: Gabriel Senay

Received: 16 January 2024

Revised: 23 March 2024

Accepted: 27 March 2024

Published: 29 March 2024



Copyright: © 2024 by the authors. Licensee MDPI, Basel, Switzerland. This article is an open access article distributed under the terms and conditions of the Creative Commons Attribution (CC BY) license (<https://creativecommons.org/licenses/by/4.0/>).

1. Introduction

Extreme rainfall events worldwide occur frequently, which can be conceived of as the one of major impacts generated by these interacting physical and societal mechanisms [1]. Physical drivers, for instance, are shaped by global warming and atmospheric circulation, while societal forces are composed of rapid urbanization, impervious land, and infrastructural networks [2–5]. The complexity of interacting mechanisms has caused the frequent occurrence of extreme rainfall events and significant economic losses and casualties [6], including in Germany (13 July 2021), Pakistan (June 2022), Pennsylvania (2023), and Libya (September 2023). In China, extreme rainstorms have also been frequent, notable one in Zhengzhou on 20 July 2021, which caused over 380 casualties and garnered widespread attention [7]. Developing countries have limited practical experience and infrastructure for urban waterlogging control, leading to more challenges in mitigating waterlogging during frequent extreme rainstorms than in developed countries.

Considering the limited land availability, many countries have proposed flood risk assessment methods [8] and urban waterlogging control measures [9], including America's Best Management Practices (BMP) [10], Low Impact Development (LID) [11], and Green Infrastructure (GI) [12]; Britain's Sustainable Urban Drainage Systems (SUDs) [13]; Australia's Water Sensitive Urban Design (WUDs) [14]; New Zealand's Low Impact Urban Design and Development (LIUDD) [15]; and China's Sponge City [16]. Most of the above measures are small-scale and dispersed green infrastructures at the source, demonstrating

remarkable effectiveness in reducing rainwater and pollution load during light rainstorms but exhibiting limitations in heavy rainstorms. Additionally, the mountainous land availability for LIDs is restricted and it is focused on infiltration and detention; considering the large slope variation and frequent flash floods, pumping stations and storage tanks are necessary to be applied.

Heavy rainfall and large slope variations in mountainous areas intensify scouring and non-point source pollution, making storage tanks essential for reducing peak runoff and pollution. Some researchers indicate that sewer sediments in urban pipelines lead to high-concentration overflow pollution [17,18]. The “Overflow Peak Pollution Interception” (OPPI) method, addressing both water quality and quantity in overflow situations, has been proposed for designing storage tanks [19]. However, there is a noticeable lack of studies specifically focusing on drainage efficiency in this context. Combining storage tanks with pumping stations proves effective and economical, especially considering land use and construction costs. Research suggests that vertical combinations of up-pumping stations and down tanks are notably effective, but limited underground space requires consideration, shifting the focus to the scale of storage facilities. American and British storage volume formulas, based on the water balance principle and mathematical algorithms like the finite difference method and continuous rainfall time series, are widely used [20,21]. However, these formula calculations can lead to significant errors. The development of urban stormwater models like the Storm Water Management Model (SWMM) and Inforworks has made them popular for scale simulation [22,23]. One study [24] used the Inforworks model to design four scales of pumping stations, optimizing them with the deprivation coefficient method and calculating the effective storage tank volume using the rainfall depth method. Overall, while most studies design storage pumping stations based on a specific rainwater volume, the regional scope has expanded to include watersheds, extending rainwater collection time and increasing drainage pressure. Storage pumping stations are effective in rapid drainage and flood peak reduction, but the reduction of water volume requires source control. So, the combination measures of storage pumping stations and LIDs need to be considered, but recent research focuses on the optimization of LID.

LIDs are viewed as a promising strategy for controlling urban waterlogging and ecosystem pollution [24]. Initially, research concentrated on experiments and identifying suitable areas for implementing a single LID [25]. Subsequently, urban flood models, particularly the open-source Storm Water Management Model (SWMM), were used for quantitative analysis of LID’s effects [26]. The focus of subsequent studies shifted from a single LID to a combination of LIDs [27,28]. Furthermore, the spatial layout of LIDs is a critical aspect of engineering construction. Research has shown that dispersed LID implementations can effectively reduce surface runoff and pollution [29,30]. The results were consistent with the study [31]. Considering the limited land use in mountainous areas, dispersed LID implementation was not feasible. Therefore, while the potential for LID implementation based on upstream–downstream relationships has been discussed, actual research on this is rare [32,33]. To address these challenges, including the differences between upstream and downstream areas and flash floods, a comprehensive “source reduction–process control–end treatment” framework integrating LIDs and storage pumping stations is being explored.

The above-mentioned research focused on optimizing LID and pumping stations separately from scale design and spatial layout [24,25]. However, few studies have combined both. Further, there is little research on the rainwater drainage network distribution. It is very valuable for dividing drainage areas based on regional terrain characteristics. However, some research just focuses on water distribution network partitioning and optimizing based on simultaneous cost and energy optimization [34–36]. Therefore, the main contributions of this work are as follows: (1) Proposing a reduction–process control–end treatment framework, coupling storage pumping stations and LIDs, for reducing urban waterlogging. (2) Designing various combination schemes based on upstream–downstream relationships and waterlogging point distribution, selecting the best solution using different runoff indicators. The analysis extends the understanding of runoff control through

LIDs and storage pumping station coupling, filling gaps in previous research and offering insights for urban construction in developing countries.

2. Materials and Methods

2.1. Framework

Based on the characteristics of flash floods and high flood peaks in mountainous areas, we proposed a source reduction–process control–end treatment framework composed of storage pumping stations and LIDs, as shown in Figure 1. The framework consists of three systems: the source LID system, the drainage network, and the storage pumping stations. The LID system integrates decentralized green infrastructure components to reduce surface runoff volume and pollution at the source, easing the pressure on the pipeline network. The drainage network system collects and transports surface runoff and the storage pumping stations drain at the end. During drainage, rainwater acts as the key link connecting different components of the system. LIDs have limited capacity to regulate and store rainwater. Residual rainwater, which acts as a lower boundary condition for discharge, significantly impacts pipeline network design. However, when discharge exceeds the drainage network’s design standards, urban waterlogging, as a lower boundary condition, determines the capacity of storage tanks and pumping stations. Additionally, pollution concentration, another critical factor, is similarly considered in this framework.

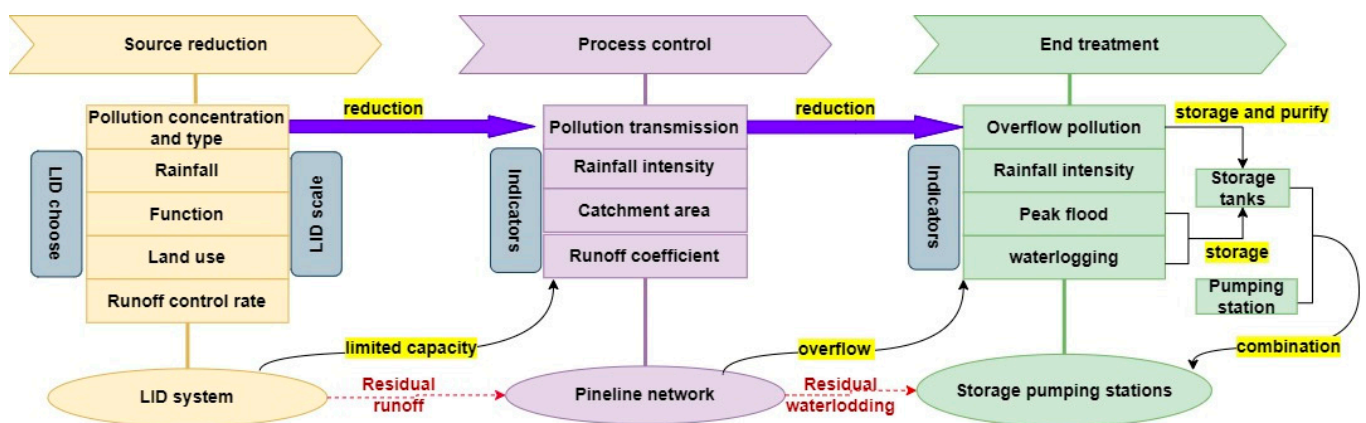


Figure 1. The source reduction–process control–end treatment framework.

This framework has a better effect when applied in areas with significant terrain changes and upstream and downstream relationships. So, the effectiveness of this framework was demonstrated in a case study in Yi County, Hebei Province, China, focusing only on water quantity due to the absence of water quality data.

2.2. Study Area

Yi County located in northern Taihang mountain, in Hebei Province, China, with 70% mountainous and hilly areas, was adopted as the case study. The region belongs to the warm temperate continental monsoon climate with an average annual precipitation of about 560 mm. The rainfall displays an uneven characteristic, mainly focusing on summer. The case study (115°28′~115°32′E, 39°19′~39°21′N) is surrounded by the North Yishui River and the Line of South-to-North Water Diversion, which has a total area of 1200.01 km², as shown in Figure 1, including 33% residential land, 26% commercial land, 18% roads, 14% green land, and 10% industrial land. The slope changes significantly, with a maximum slope value of 22.72% and an average slope of 5.01% (Figure 2). The topography gradually descends from northwest to southeast, leading to notable variations in water flow levels and a higher risk of inundation.

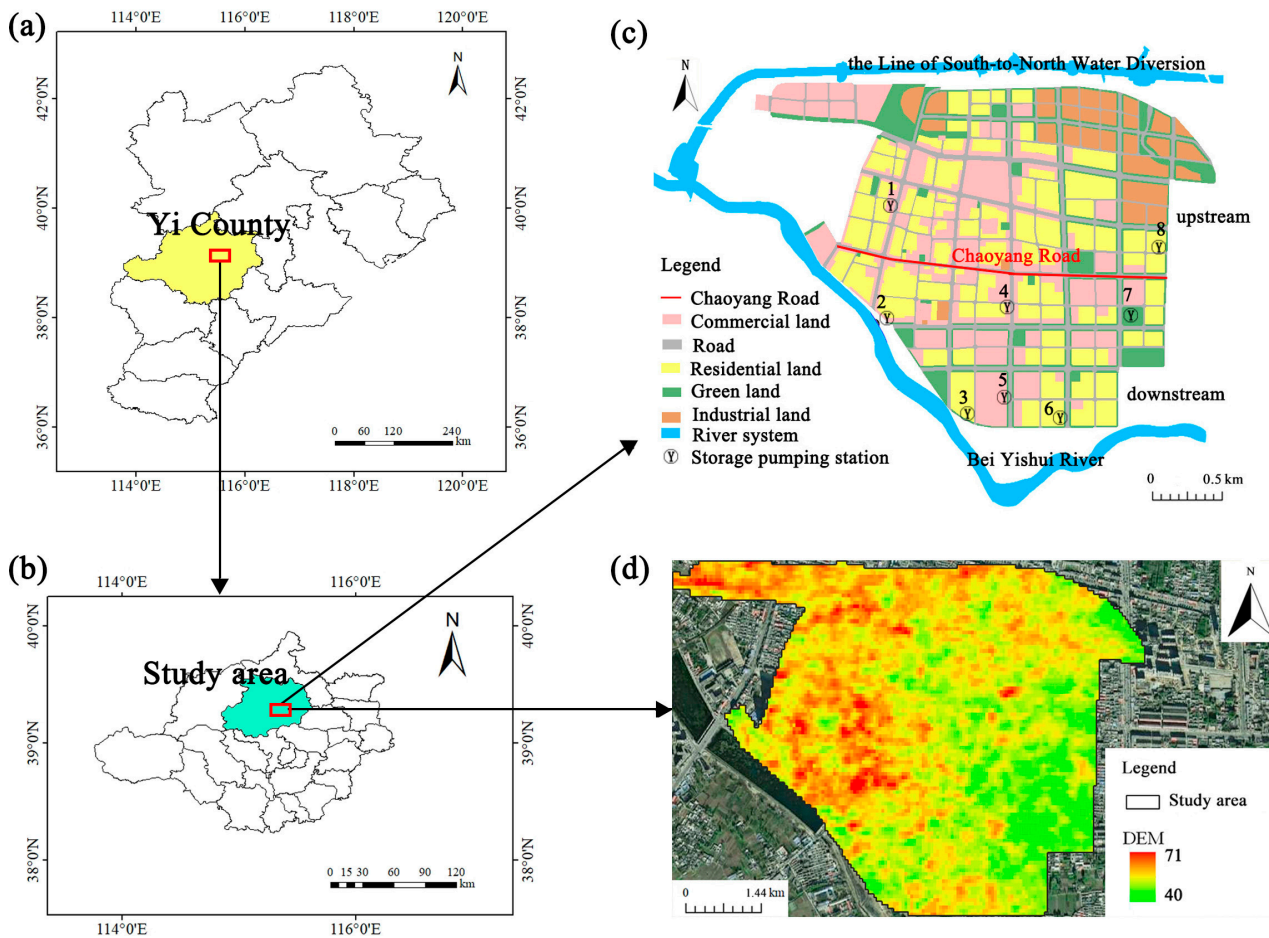


Figure 2. The schematic diagrams of the (a) Yi County location, (b) study area location, (c) land use types of the study area and distribution with storage pumping stations 1 to 8, and (d) DEM.

2.3. Data Sources

2.3.1. Data for Modeling

To establish the model of the study area, Digital Elevation Model (DEM) and land use data were collected for sub-catchment delineation. The pipeline network was digitized from pipe network data, and the model was calibrated and validated using precipitation and waterlogging data. DEM with a spatial resolution of 30 m was downloaded from the Geospatial Data Cloud website (<https://www.gscloud.cn/> (accessed on 1 April 2023)). The land use and pipe network data were obtained from Norendar International Ltd. Baoding, China. Precipitation data were obtained from The Bureau of Hydrology and Water Resources Survey of Baoding. Waterlogging data was obtained from the site survey. Table A1 displays the detailed data sources and their usage required for the modeling process.

2.3.2. Waterlogging Site Survey

The extreme rainfall event in Yi County on 19 July 2016 caused extensive waterlogging and the distribution of severe waterlogging points was determined based on remote sensing images. To survey the waterlogging situation in this study area, the site survey was conducted in Yi County in July 2019, identifying eleven representative points chosen based on topography and the distribution of waterlogging, as illustrated in Figure 3. Two waterlogging monitoring experiments were conducted on 21 July 2019 and 12 July 2020, based on weather forecasts. The first rainfall event lasted 7 h with a total of 27 mm, and the second rainfall event lasted 9 h and had an average intensity. We monitored and recorded the process of road waterlogging and its maximum depth of waterlogging while measuring

the extent of inundation and the recession time. The maximum waterlogging depth at the eleven points was calculated by averaging measurements taken near each point using a box ruler [37]. Relevant data is shown in Figure 4.



Figure 3. Distribution of survey waterlogging points.

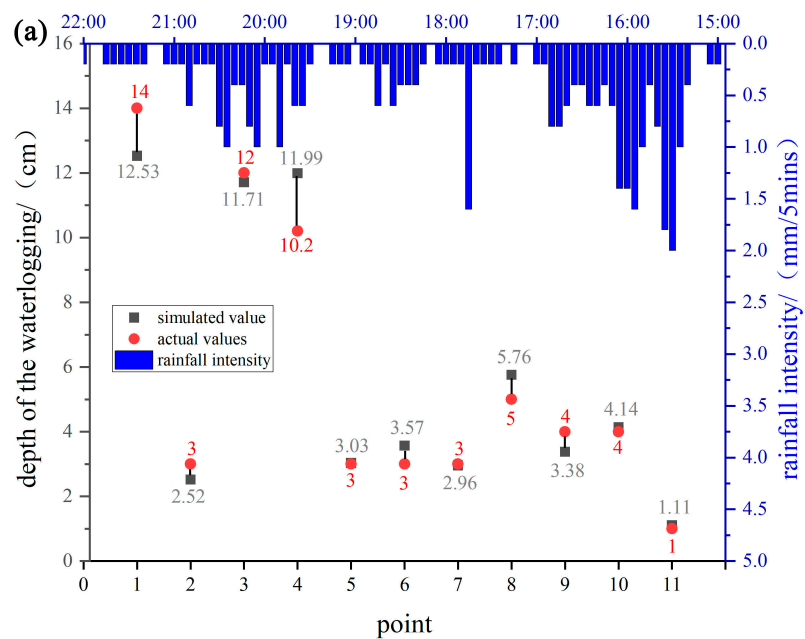


Figure 4. Cont.

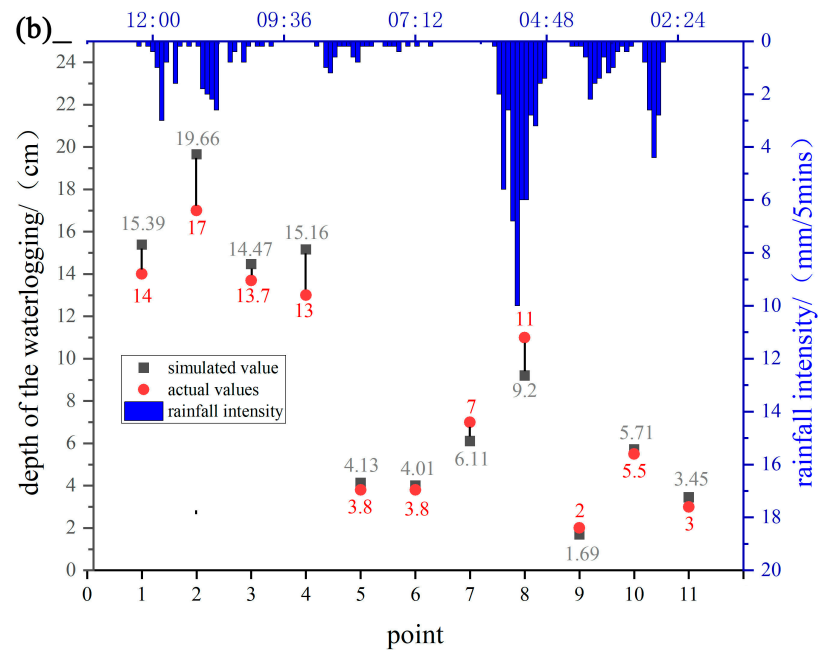


Figure 4. Simulated and measured values of maximum waterlogging depth under (a) “7.22” rainfall event in 2019 and (b) “7.12” rainfall event in 2020.

2.4. Remote Sensing

The calibration and validation of maximum waterlogging depth in SWMM accounted for extreme values, despite local disturbances. Nowadays, many studies use remote sensing images to simulate precipitation and urban flooding [38–40]. Consequently, remote sensing (RS) was employed to determine the extent of inundation, compared with the SWMM [41].

2.4.1. Data Preprocessing

To accurately obtain the waterlogging extent of the study area, Sentinel-2 imagery with a spatial resolution of 10 m was downloaded from the European Space Agency’s official website (<http://scihub.copernicus.eu/> (accessed on 1 April 2023)), and the 30 m resolution SRTM-1 Digital Elevation Model (DEM) data were downloaded from the Geospatial Data Cloud Platform [42,43]. Image processing was conducted using the SNAP 8.0 software’s resampling tool to adjust Sentinel-2 data to a 10 m wavelength and resolution, and the images were synthesized using EVNI 5.3.

2.4.2. Image Feature Extraction

The Region of Interest (ROI) is utilized for the classification of remote sensing images, with the Jeffries–Matusita method assessing the degree of difference in training sample separation. Simulation result accuracy was determined using the Nash–Sutcliffe Efficiency coefficient (NSE), which varies between 0 and 2. A Jeffries–Matusita value above 1.8 indicates significant differences and strong separability between the two samples. A Jeffries–Matusita value between 1.4 and 1.8 suggests reduced differences and weaker separability between samples. A Jeffries–Matusita value below 1.4 implies insignificant differences between samples, necessitating their division and resampling. A Jeffries–Matusita value under 1 indicates that the samples should be merged into the same category. Its calculation formula is as follows:

$$J_{mn} = \left\{ \int x \left[\sqrt{p(x/m)} - \sqrt{p(x/n)} \right]^2 dx \right\}^{\frac{1}{2}} \quad (1)$$

where J_{mn} represents Jeffries–Matusita. $\sqrt{p(x/m)}$ represents the conditional probability of any pixel x appearing in class m in the image. $\sqrt{p(x/n)}$ represents the conditional probability of any pixel x appearing in class n in the image.

Using downloaded Sentinel-2 images and site survey data, land use types were classified via indoor visual interpretation, with specific samples chosen as training data. ROI separability was calculated until the Jeffries–Matusita parameter exceeded 1.8. The maximum likelihood classification method was employed for these samples, with the Kappa coefficient serving as an indicator of classification accuracy in ENVI 5.3 [3]. Its calculation formula is as follows:

$$Kappa = \frac{M \times \sum_{i=1}^n X_{ii} - \sum_{i=1}^n (X_{i+} \times X_{+i})}{M^2 - \sum_{i=1}^n (X_{i+} \times X_{+i})} \quad (2)$$

where $Kappa$ represents the accuracy evaluation index. M represents the total number of samples extracted from the area. N represents the total number of land use types divided. i represents quantity ($i = 0, 1, 2, \dots, n$). X_{ii} represents the value on the corner line. X_{i+} and X_{+i} , respectively, represent the partition classification in the confusion matrix the sum of columns and rows.

2.5. SWMM

2.5.1. Model Setup

SWMM as an open source and free urban flood model, was initially proposed in 1971 and had upgraded SWMM 5.2. SWMM was widely used. It was chosen for this study due to its ability to simulate LIDs, storage pumping stations, and other relevant features. Runoff generation and sink flow processes were modeled separately using the nonlinear reservoir routing method and the de Saint-Venant equations. Additionally, infiltration was simulated through the application of the Horton method [44]. Eventually, this study area was generalized into 4 drainage zones, 351 sub-catchments, 196 nodes, 196 pipelines, and 4 drainage outlets by using the above data (Figure 5).

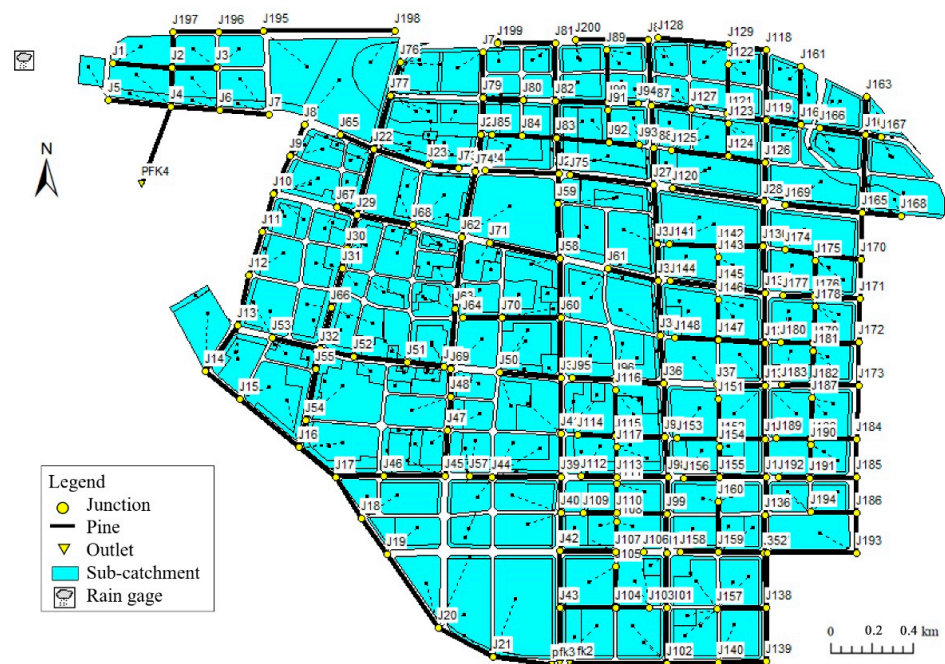


Figure 5. Generalization diagram of the SWMM for the study area.

2.5.2. Calibration and Validation

Calibration and validation are vital for model simulation. In areas lacking the monitoring flow data, the comprehensive runoff coefficient method and the maximum depth of surface water accumulation method are widely used [45,46]. The former emphasizes the adjustment of non-deterministic parameters, guided by the empirical value range in diverse regions until the targeted value of the comprehensive runoff coefficient is reached [47,48]. The latter emphasizes that parameters are adjusted according to the relative error between simulated and measured values. In particular, simulated values of waterlogging depth are calculated by evenly distributing the maximum overflow of waterlogging points obtained from SWMM to nearby streets. The relative error is calculated by Equation (3).

$$\text{Relative error} = \frac{H_1 - H_2}{H_1} \times 100\% \quad (3)$$

where H_1 represents the measured value of waterlogging (cm), and H_2 represents the simulated value of waterlogging (cm).

The study area belongs to the central urban area with dense buildings. According to the above methods, the comprehensive runoff coefficient was calculated as 0.692 based on land use type. Non-deterministic parameters were adjusted multiple times until reaching this target value. Then, we calculated the error between simulated and measured values of maximum waterlogging depth under two rainfall events. The results indicated that the error of each waterlogging point was within 20%, which means the model performed well (Figure 6). The parameter values are shown in Table A2.

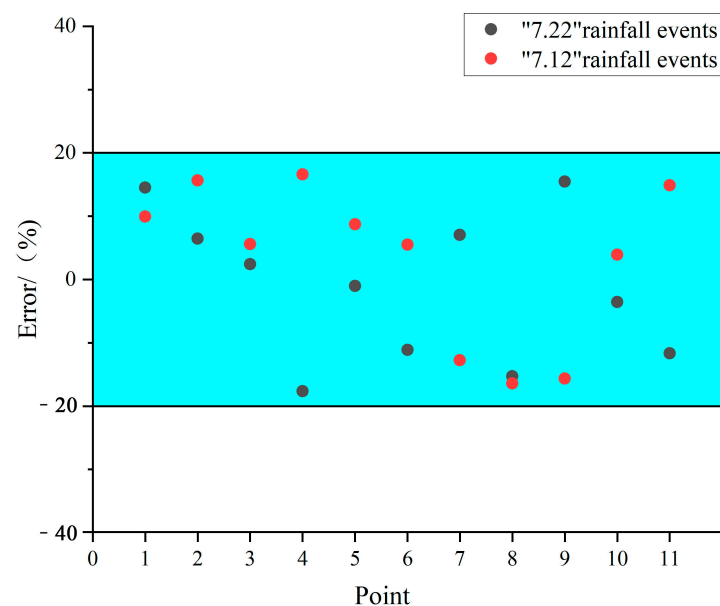


Figure 6. The relative error between the simulated and observed maximum waterlogging depths during the two rainfall events.

The above methods compared the simulated and measured values of maximum waterlogging depth. Due to the limited accuracy data, it is not possible to accurately identify changes in road waterlogging depth, but it can reflect the inundation ranges. So, we used remote sensing to compare the inundation ranges derived from remote sensing images with those from SWMM. The categorization of the area was clear, encompassing buildings, roads, and water bodies. Jeffries–Matusita scores of 1.813 and 1.827 indicate strong sample separation and clear differentiation. This level of sample separation meets differential evaluation requirements, confirming the sample selection’s adequacy. For visual comprehension of its distribution, the maximum likelihood classification method was used to generate a figure. Figure 7a,b show that the waterlogging distribution is relatively

concentrated in the southwest and dispersed in the northeast. The results revealed that the waterlogging areas during the two rainfall events were 22% and 17%, respectively. The former rainfall events generated bigger inundation ranges, which also indicates that rainfall intensity affects inundation ranges. The results of the SWMM (Figure 8) indicate that the waterlogging areas under two rainfall events are 19.8% and 16.2%, respectively, which is consistent with the results obtained from remote sensing images. Due to the limited accuracy, the changes in the accumulated depth of waterlogging cannot be obtained by remote sensing images, but the maximum overflow of waterlogging points obtained from SWMM is similar to measured values. Therefore, the waterlogging distribution in the main urban area is consistent with SWMM and monitoring data, which indicates that the SWMM model has good accuracy.

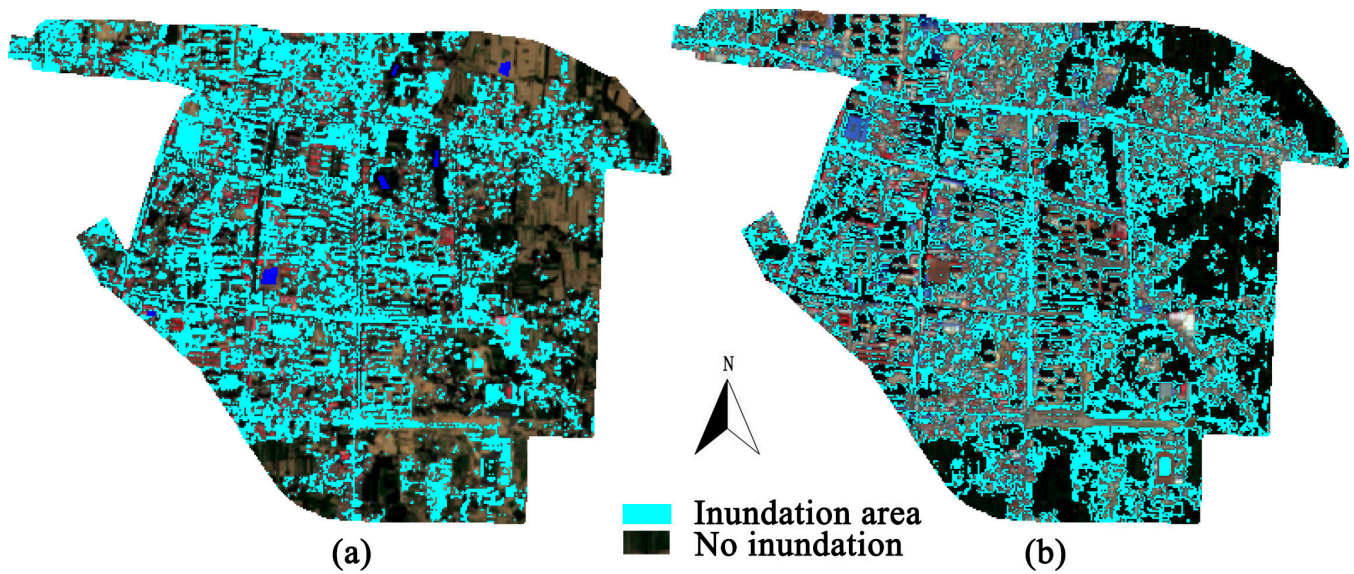


Figure 7. Distribution of inundated areas: (a) remote sensing images on 21 July 2019; (b) remote sensing images on 12 July 2020.

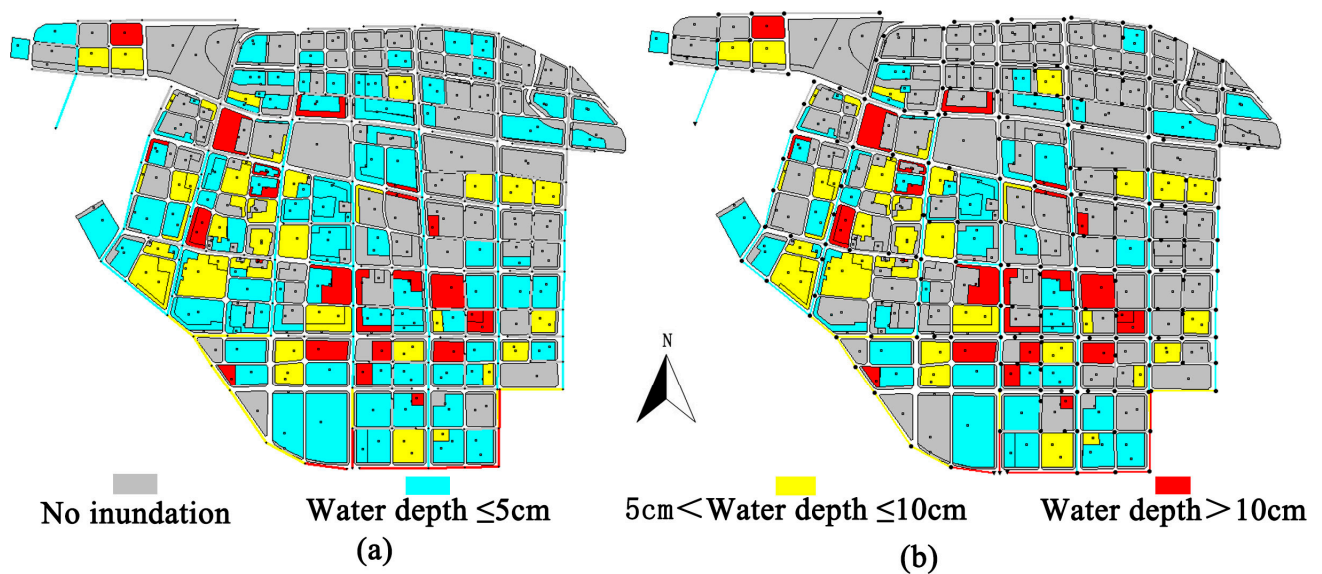


Figure 8. Distribution of inundated areas: (a) SWMM results on 21 July 2019; (b) SWMM results on 12 July 2020.

2.5.3. Design Rainfall

Rainfall was designed for return periods of 2, 5, 10, and 20 years referring to topography and design standards of pipe networks and pumping stations in Yi County. The rainfall intensities of a two-hour duration were calculated based on the Chicago design storm method [49], and the Baoding rainstorm formula Equation (4), which are shown in Figure 9.

$$i = \frac{14.973(1 + 0.6856 \lg P)}{(t + 13.877)^{0.776}} \quad (4)$$

where i represents rainfall intensity (mm/min), P represents rainfall return period (year), and t represents rainfall duration (min).

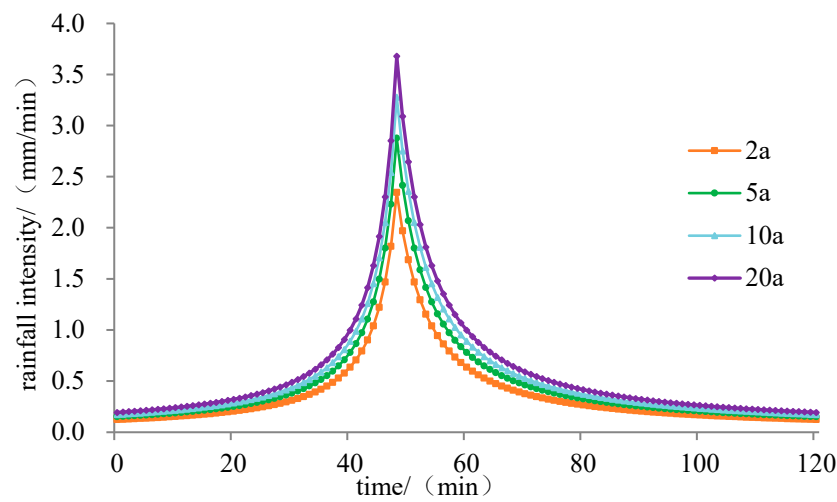


Figure 9. Synthetic hyetograph of the design rainfalls for the return periods of 2, 5, 10, and 20 years.

2.5.4. LID Implementation

LID is an ecological technology system that can easily achieve urban rainwater collection and utilization. Land use type and suitable construction area are usually considered for LID implementation. The most common LID measures are permeable pavements, infiltration trenches, sunken greenbelts, rain gardens, green roofs, and rain barrels [45]. Permeable pavements, preferred for their permeability and aesthetics over infiltration trenches, are widely used in sidewalks and parking lots. Sunken greenbelts and rain gardens excel in rainwater retention; however, rain gardens, with higher maintenance costs, are typically used in upscale residential areas. Green roofs are ideal for buildings with strong roof-bearing capacity, while rain barrels are the preferred choice for collecting roof rainwater. Overall, considering Yi County's land use and older buildings, the decision was made to use permeable pavements in residential and commercial areas, sunken greenbelts in green spaces, and rain barrels for roof rainwater collection. The results of LID parameters referring to related articles like [47–50] were shown in Table A3.

2.5.5. Storage Pumping Station Setup

Storage tanks can delay and reduce flood peaks by retaining rainwater in urban areas. When combined with pumping stations, they offer the benefits of reduced construction scale and rapid drainage in low-lying areas. The smaller diameters of downstream pipes, as indicated by pipe network data and drainage conditions, lack capacity for upstream rainwater. Consequently, eight storage pumping stations were established near outfalls and severe waterlogging locations, depicted in Figure 2. Taking into account the extensive land use and dense population in residential and commercial areas, green spaces and squares were generally prioritized.

The effective volume of the storage tanks is critical, influencing their construction scale and size. In China, the deprivation coefficient method is widely used due to the lack of pipe

network flow data [23]. At present, the design return period of the rainwater pipe networks is 2 years. To enhance the drainage standards, a 10-year design return period was used for determining the scale of storage pumping stations. First, the discharge coefficient was calculated as 0.693, 0.677, 0.676, 0.681, 0.663, 0.680, 0.689, and 0.658, respectively, based on its definition. Then, the results were substituted into Equation (5) to calculate the effective volume of eight storage tanks. To enhance design safety, the volumes of the eight storage tanks were increased to 500 m³, 1200 m³, 2500 m³, 1000 m³, 1000 m³, 1250 m³, 800 m³, and 600 m³. Considering the limited land use and construction difficulty, the rectangular storage tanks were selected, and their depth was 2 m, 3 m, 2.5 m, 2 m, 2.5 m, 2.5 m, 2 m, and 3 m.

$$V = \left[-\left(\frac{0.65}{n^{1.2}} + \frac{b}{t} \frac{0.5}{n + 0.2} + 1.10 \right) \log(\alpha + 0.3) + \frac{0.215}{n^{0.15}} \right] Q_i t \quad (5)$$

where V represents the volume of the storage tanks (m³), α represents the deprivation coefficient (downstream design flow of storage facilities divided by upstream design flow), Q represents the upstream design flow of the storage tank (m³/min), b and n represents rainstorm intensity parameters, and t represents confluence duration (min).

Setting relevant parameters for the front tanks of pumping stations and their pumps is essential. SWMM is commonly employed when data are lacking. In this study, the scale of the pumping stations was determined by simulating surface overflow changes for a 10-year return period, and validated for a 20-year return period. SWMM offers five pump types and four pump curve options; type 3 and its corresponding curves were chosen for their ability to reflect flow variation with head [48,51]. Parameters like pump type and design flow were determined based on the relevant literature [52]. The control areas for the storage pumping stations 1 to 8 were calculated as 0.171 km², 0.107 km², 0.133 km², 0.116 km², 0.057 km², 0.072 km², 0.048 km², and 0.062 km², respectively. Based on the design flow of storage tanks, the AmacanPA 41000-700/160 8UTG1 pump sourced from Laverton North, Australia was chosen for storage pumping stations 1 to 4, and the 600ZQB-100 submersible pump for stations 5 to 8 [52]. For reliable operation, each storage pumping station was equipped with two pumps of the same type, including a backup pump. At the same time, based on the principle that the depth of waterlogging cannot exceed 0.15 m for a 10-year return period, the startup and shutoff depths of each storage pumping station are displayed in Table 1.

Table 1. Startup and shutoff depth of the storage pumping stations.

Storage Pumping Station	Startup Depth/(m)	Shutoff Depth/(m)	Maximum Depth of Surface Waterlogging/(m)	
			10-Year Return Period	20-Year Return Period
1	1.4	0.7	0.10	0.11
2	1.4	0.5	0.06	0.07
3	2.2	0.8	0	0.00
4	1.3	0.6	0.12	0.13
5	1.7	0.6	0	0.01
6	1.2	0.7	0.11	0.14
7	1.2	0.5	0.02	0.04
8	1.3	0.7	0	0.00

2.5.6. Design Schemes

The study area was divided to compare runoff response mechanisms among LIDs implemented upstream, downstream, and throughout the entire area, ensuring similar control areas for both upstream and downstream LIDs. Considering significant topographical changes, land use types, and the orientation of the pipeline network, the area north of Chaoyang Road was designated as upstream (722.06 ha) and the south as downstream (477.95 ha), as shown in Figure 2. It was crucial to combine the three selected LIDs with 10% permeable pavements for residential and commercial areas, 60% sunken greenbelts

for green land, and 1046 rainwater buckets (526 upstream and 520 downstream) near the building. LIDs were then implemented separately upstream, downstream, and in the entire area, creating three different spatial layouts. Three new schemes were formed by integrating LIDs with eight storage pumping stations. The control areas of a single LID and multiple LIDs were similar, both upstream and downstream. The six schemes are shown in Figure 10. Schemes 1 to 3 are only implemented LIDs separately upstream, downstream, and the whole area. Schemes 4 to 6 are based on the first three schemes and combined with eight storage pumping stations.

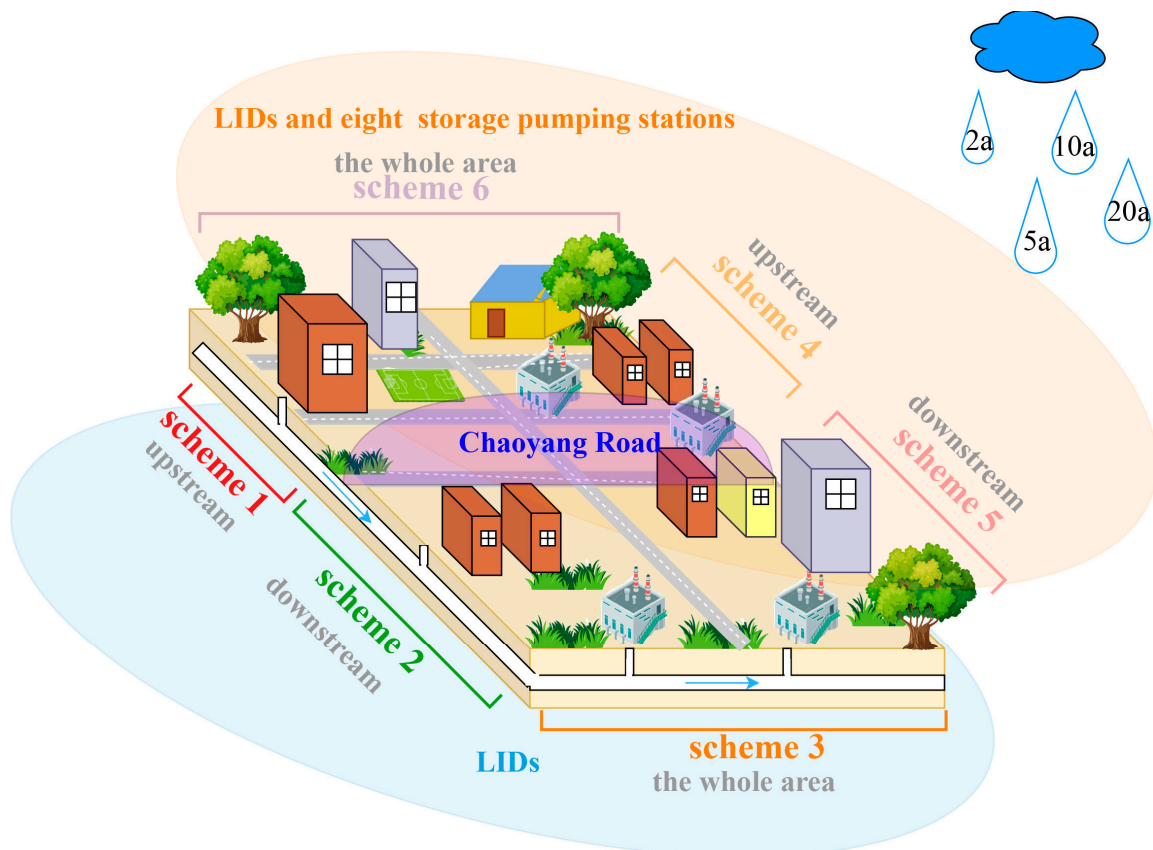


Figure 10. Schematic diagram of six schemes.

3. Results

3.1. Surface Runoff Reduction

The effect of each scheme in mitigating the amount of runoff is presented in Figure 11. Scheme 1 reduces runoff by 33.47% to 34.76% and Scheme 2 by 32.43% to 32.71% during four rainfall return periods. Scheme 3, with a runoff reduction of 66.12% to 68.10%, performed the best. However, integrating storage pumping stations (Schemes 4 to 6) had a minimal impact on runoff reduction compared to Schemes 1 to 3. Overall, LID measures, implemented either upstream or downstream, demonstrated similar runoff reduction effects within the same return period. Notably, the cumulative effect of implementing LID measures across the entire area was roughly equal to the combined impact of separate upstream and downstream implementations. This suggests that storage pumping stations have a limited impact on reducing runoff. Additionally, it is important to note that each scheme's performance declined with longer return periods.

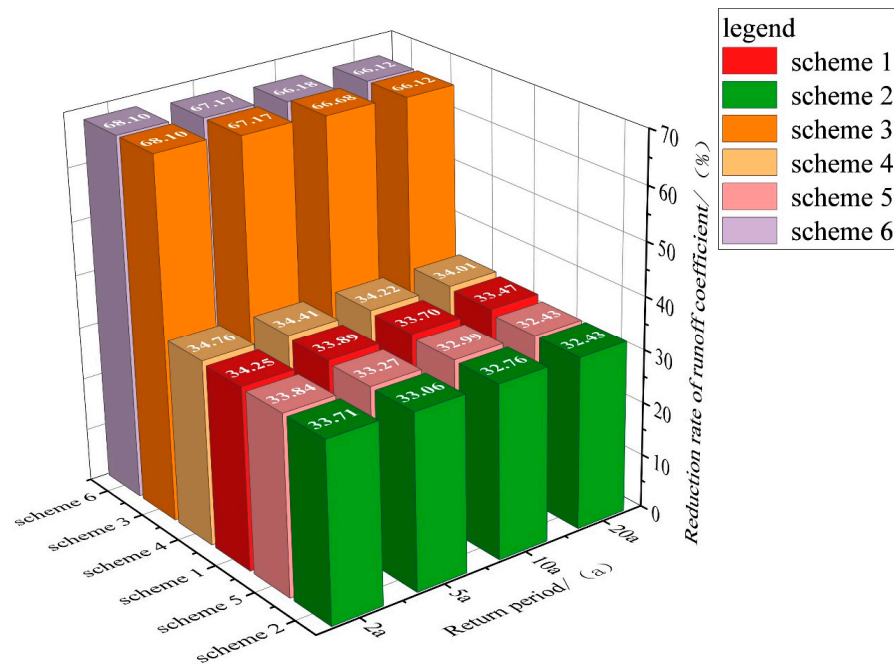


Figure 11. Reduction rate of runoff coefficient under six schemes for the return periods of 2, 5, 10, and 20 years.

3.2. Peak Outflow Reduction

Peak outflow reduction varied among different scenarios, as shown in Figure 12. Scheme 1 achieved a peak runoff reduction of only 8.46% for a 2-year return period. However, Scheme 2's peak outflow reduction, ranging from 40.83% to 48.97%, significantly surpassed Scheme 1's across rainfall return periods of 2 to 20 years.

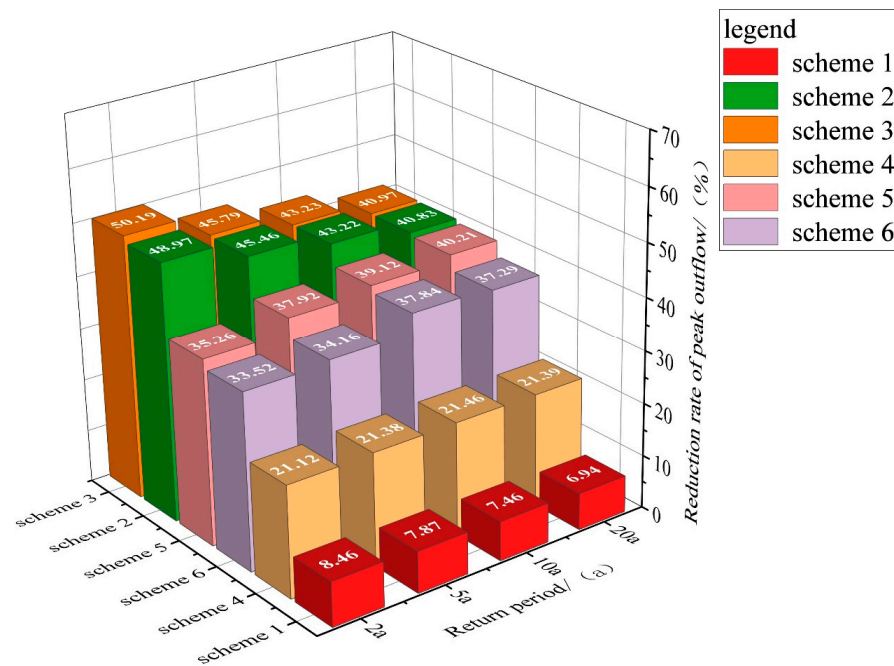


Figure 12. Reduction rate of peak outflow under six schemes for the return periods of 2, 5, 10, and 20 years.

Scheme 3 showed a peak runoff reduction between 40.97% and 50.19%, comparable to Scheme 2's performance. Notably, the effectiveness of Schemes 1 to 3 decreased with

longer return periods. When analyzing schemes with storage pumping stations, peak outflow reductions were 21.12% to 21.39% for Scheme 4, 35.26% to 40.21% for Scheme 5, and 33.52% to 37.29% for Scheme 6. Particularly, Scheme 4's peak outflow reduction, after implementing storage pumping stations, was over triple that of Scheme 1. Despite reduced effectiveness in Schemes 5 and 6, their peak outflow reduction rates remained above 30%. Interestingly, Schemes 4 to 6 showed increasing impact with longer return periods, except for a slight decrease in the 20-year period due to the scale limitations of the storage pumping stations.

3.3. Peak Time of Outflow

The peak time of outflow under six schemes for different rainfall return periods is listed in Table 2. It indicated that LIDs and storage pumping stations could delay the peak time, although this time shifted earlier as the return periods increased. Schemes 2 and 3 showed better capacity to delay peak times than Scheme 1, but their impact on extending waterlogging mitigation periods was not significantly greater. After implementing storage pumping stations, the peak time could be delayed by 6 to 26 min, 28 to 51 min, and 16 to 32 min, respectively, for Schemes 4 to 6. Overall, storage pumping stations played a more significant role in delaying the peak time of outflow, especially for Scheme 4, which had the best effect. In addition, the performance in each scheme decreased as the return periods increased.

Table 2. The occurrent time of peak outflow under no measures and six schemes in different return periods.

Measures	2a	5a	10a	20a
no measures	52 min	52 min	52 min	52 min
Scheme 1	54 min	54 min	53 min	53 min
Scheme 2	57 min	56 min	55 min	54 min
Scheme 3	61 min	57 min	55 min	54 min
Scheme 4	75 min	79 min	66 min	57 min
Scheme 5	103 min	91 min	86 min	79 min
Scheme 6	84 min	75 min	77 min	67 min

3.4. Outflow Process

Figure 13 shows the outflow change process under different return periods, with each scheme's variation trend being relatively consistent across these periods. All schemes contributed to reducing both outflow and drainage time. Regarding outflow reduction, Scheme 3 was most effective in each return period. Scheme 2 outperformed Scheme 1 pre-rainfall but was less effective post-rainfall, with inflection points at 17.2, 21.3, 24.2, and 27.1 h for 2, 5, 10, and 20-year return periods, respectively. From the drainage time reduction perspective, it was longer with each scheme as the return periods increased. Scheme 3 had the shortest drainage time, followed by Scheme 2, with a marginal difference of only 3 h. Compared to Schemes 1 to 3, implementing storage pumping stations (Schemes 4 to 6) reduced the entire process's outflow value to below 6500 L/s. It indicated that storage pumping stations had the ability to stagger and reduce outflow. In addition, the change frequency of outflow increased due to the increase in the frequency of storage pumping stations opening and closing, but the drainage time was reduced significantly.

SWMM simulation results indicated that most pipelines were emptied within the first six hours of drainage. Instances of pipeline overload and surface waterlogging were rare. However, downstream pipelines with small diameters and gentle slopes retained rainwater, leading to low outflow at the outlet and longer drainage times. Considering the residual outflow and complex outflow changes could increase the risk of pipeline overload within the first six hours, an in-depth analysis of the outflow process for Schemes 1 to 6 will be conducted.

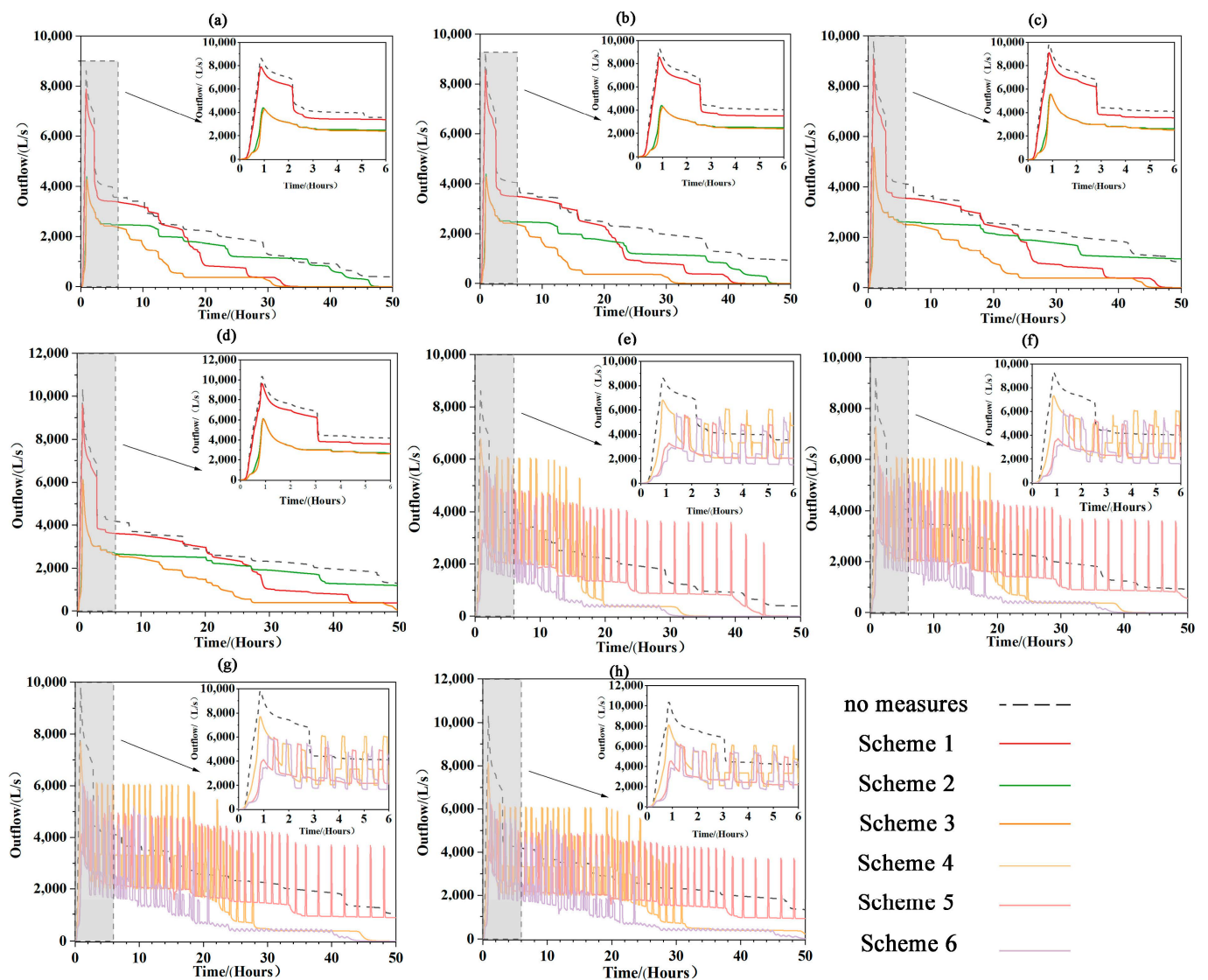


Figure 13. Outflow process of Schemes 1 to 3 for the return periods of (a) 2a, (b) 5a, (c) 10a, (d) 20a and Schemes 4 to 6 for the return periods of (e) 2a, (f) 5a, (g) 10a, (h) 20a.

The outflow trend with Scheme 1 was similar to that without any measures, but it slightly reduced outflow. The outflow change under Scheme 3 occurred in three stages, with a significant reduction effect, particularly in the second stage, reaching about 50%. Scheme 3, compared to Scheme 2, had a similar outflow trend but was more effective in reducing outflow. In addition, implementing LIDs and storage pumping stations could stagger and reduce outflow, having a beneficial impact on controlling outflow below 6000 L/s and shortening the overload time of pipelines. Scheme 5's outflow curve was the most regular, varying between 2200 and 2600 L/s for most of the time, with high-speed duration not exceeding one hour. Although Scheme 5's curve changes were complex, it had lower outflow. Compared to Schemes 5 and 6, Scheme 4's curve changes were more complex. Overall, storage pumping stations significantly alleviated pipeline overload pressure and reduced outflow in the first six hours of drainage.

3.5. Scheme Selection

Based on the above results, it was evident that different schemes had varying degrees of impact on different indicators. To thoroughly evaluate each indicator, the performances of the six schemes were initially ranked (Figure 14), followed by comparing their impacts to select the optimal scheme.

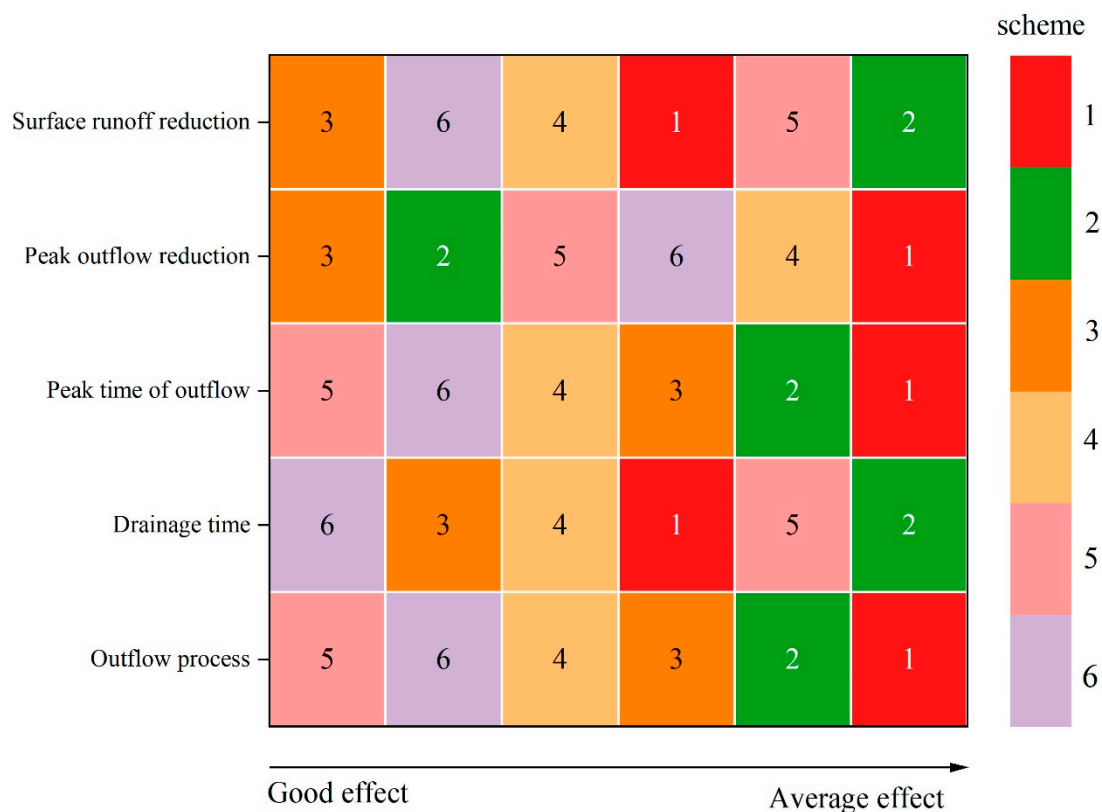


Figure 14. Prioritize the effects of six schemes on surface runoff reduction, peak outflow reduction, peak time of outflow, drainage time, and outflow process.

Optimization was performed using the exclusion method based on sorting results. Given that peak outflow factors are more critical than runoff volume in urban flood warnings, the primary focus was on reducing peak outflow and delaying peak time. Schemes 1 and 4 were first excluded due to their minimal impact on peak outflow reduction, with rates less than 22%. Similarly, Schemes 2 and 3 were excluded for their limited ability to delay peak times. Comparing Schemes 5 and 6, Scheme 5 showed significantly better performance in peak runoff reduction, peak time delay, and outflow process, making it more valuable for flood control and pipeline pressure relief. Although Scheme 5 had a lower surface runoff reduction rate, it still reached about 30%. Meanwhile, the differences in drainage time between them were only 10 h. Moreover, the study area is part of an old urban region where a drainage project was recently completed. Implementing LIDs throughout the area posed greater challenges than installing storage pumping stations along the river. After a rough comparison of economic costs, Scheme 5 was eventually chosen.

4. Discussion

In this study, a source reduction–process control–end treatment framework was proposed for reducing urban waterlogging and runoff pollution load in mountainous areas. The water quantity in this framework is applied to Yi County in Hebei Province, China, composed of storage pumping stations and LIDs. The runoff control effects of six schemes were analyzed through various indicators, as illustrated in Figures 9–12 and Table 2. Schemes combining LIDs with storage pumping stations modified the outflow process, resulting in peak time delays of 3 to 51 min. Unlike LID-only schemes, these combinations notably eased pipeline overload pressure, with similar effects on reducing surface runoff. In particular, Scheme 4, integrating storage pumping stations, tripled the peak outflow reduction rate compared to Scheme 1. Conversely, the effectiveness of Schemes 5 and 6, attributed to storage tanks, fell below that of Schemes 2 and 3. These findings underscore the signifi-

cant effectiveness of storage pumping stations in reducing peak outflow. However, their impact on reducing runoff volume was less pronounced according to established scientific standards and observations. In contrast, LIDs primarily reduce both runoff volume and peak outflow. The combined use of storage pumping stations and LIDs, as proposed, offers a synergistic advantage for managing urban waterlogging. The results were consistent with [53,54]. These studies have confirmed the feasibility of combination methods.

Six spatial layout schemes varied in their reduction of runoff volume and peak outflow. In this study, the storage pumping stations were usually implemented near outfalls and serious waterlogging points, and LIDs were implemented based on the upstream and downstream relationships. The results show that the effect of runoff reduction is similar when implementing the storing pumping stations. It means that LID measures play a major role in reducing the runoff volume and the storage pumping stations have almost no impact. The reason is that the working principles are completely different. LID measures are small-scale and dispersed green infrastructures at the source, which can directly recycle rainwater into groundwater by infiltration. But the storage pumping station stores rainwater first and then discharges it. Therefore, reducing runoff from the source mainly relies on LID measures.

The research showed that LIDs in downstream areas significantly reduce peak outflow, while LIDs' effectiveness was limited when implemented upstream in this study. The causes of these results were analyzed based on topography and existing drainage pipelines. Although LIDs extend rainfall infiltration duration and increase overall infiltration, implementing LIDs upstream is effective, but it does not extend downstream. The downstream rainwater still exceeds the drainage capacity of the downstream pipeline network during pre-rainfall. In contrast, downstream LID implementation results in rainwater retention and infiltration, especially noticeable during pre-rainfall. This not only directly reduces downstream runoff but also staggers upstream rainwater, significantly reducing peak outflow. Therefore, upstream LID implementation results in much less peak outflow reduction at discharge points compared to downstream, similar to the effect of whole-area implementation. Thus, the results indicate that the spatial location of LIDs and topography should be carefully considered.

Another result indicated that runoff reduction from LIDs, whether upstream or downstream, was similar despite the control area being the same. Implementing LIDs across the entire area was roughly equal to the combined upstream and downstream effects, suggesting that the area of implementation is more crucial than the spatial location. However, the location of LID implementation impacts peak outflow reduction differently. Upstream LIDs exhibit a reduction rate four times higher than their downstream counterparts. While the limited capacity of LIDs may not have a significant impact on delaying peak time. Implementing storage pumping stations significantly improved lag time effects and altered the outflow process. The main reason for this result may be the storage tanks. Residual rainwater stored in tanks compensates for the upstream LID shortage, reducing peak outflow—a major advantage of Scheme 4 over Scheme 1. When the water in the tanks reaches the design startup depth, pumping stations begin discharging rainwater, resulting in a lag time. Storage pumping stations gradually discharge rainwater over staggered low peak periods, altering the discharge process trend and significantly relieving pipeline network pressure.

According to this study, it can be found that LIDs' impact on runoff reduction in mountainous areas with significant slope variations and frequent flash floods is limited, necessitating the integration of storage pumping stations for efficient drainage. However, comprehensive research on this topic is still lacking. In this study, A source reduction–process control–end treatment framework is proposed for reducing urban waterlogging and runoff pollution load, coupling storage pumping stations, and LIDs. The water quantity in this framework is applied. Six schemes were designed based on regional upstream–downstream relationships and waterlogging distribution to demonstrate and apply the proposed framework. The study uniquely quantitatively analyzes the effect of different

LID schemes and their combination with storage pumping stations on runoff control. However, The study primarily focused on comparing and selecting the best scheme for runoff control effectiveness. In the future, we can employ optimization algorithms for a more thorough optimization, and refer to the optimization partitioning of the water distribution network, to help improve water network management and consider water loss [34–36]. Additionally, it is tentatively concluded that the vertical structure of up-pumping stations and down tanks can save costs, though specific data simulations are not yet available. Future research will broaden the scope of scheme optimization to include comprehensive benefits. Additionally, with limited data for calibration and validation, future efforts may involve using electronic water gauges, flow meters, and remote sensing technology to enhance measurement accuracy and frequency, as well as integrating SWMM with other two-dimensional hydrodynamic models for analyzing the overflow changes in waterlogging points. Meanwhile, the water quality of this framework could be carried out.

5. Conclusions

This study proposes a framework that couples storage pumping stations with LIDs to reduce urban waterlogging and runoff pollution, particularly in mountainous areas prone to flash floods. This combination optimizes land use and tank design by considering topography and regional upstream–downstream relationships. The water quantity of this framework is carried out and the main conclusions of this study are as follows: (1) Single LIDs are highly efficient for runoff reduction, with the implementation area being more crucial than the location. But for peak outflow reduction, downstream LIDs implementation exhibits a reduction rate four times higher than downstream counterparts. (2) Coupling storage pumping stations with LIDs significantly reduces peak outflow and delays its occurrence more than single LIDs, thanks to their rainwater storage and staggering ability. (3) The combined scheme of downstream storage pumping stations and LIDs showed the most effective outcomes in terms of runoff reduction, peak outflow reduction, occurrence timing, drainage time, and outflow process. These findings have significant implications for urban waterlogging control, taking into account regional upstream–downstream relationships and the topographical features of hilly urban areas. The framework is conducive to achieving systematic management of urban waterlogging. For urban management departments and professionals, it is possible to draw urban waterlogging risk maps for different rainfall periods based on the research results, enhancing the early warning and emergency management capabilities for responding to sudden urban waterlogging incidents. Furthermore, it can attract public attention and plan travel routes and optimal times for the public to escape.

Author Contributions: Conceptualization, Q.L.; methodology, H.L.; software, H.L.; validation, H.L. and H.Z.; formal analysis, C.G.; investigation, H.Z.; writing—original draft preparation, H.L. and Q.L.; writing—review and editing, H.L. and J.L.; funding acquisition, H.Z. All authors have read and agreed to the published version of the manuscript.

Funding: This research was funded by the National Natural Science Foundation of China (52379008, 42301015), the Postgraduate Research and Practice Innovation Program of Jiangsu Province (SJCX22_0182), and the IWHR Research and Development Support Program (WR110145B0022022).

Data Availability Statement: The data presented in this study are openly available from the Geospatial Data Cloud website (<https://www.gscloud.cn/> (accessed on 1 April 2023)), and Sentinel-2 imagery from the European Space Agency’s official website (<http://scihub.copernicus.eu/> (accessed on 1 April 2023)).

Acknowledgments: The authors gratefully acknowledge the support of various foundations and the National Cooperative Innovation Center for Water Safety and Hydro Science of Hohai University. The authors would like to thank the editor and the anonymous reviewers for their insightful comments to help us improve the quality of our papers.

Conflicts of Interest: The authors declare no conflicts of interest.

Appendix A

Table A1. Sources and utilization of data.

Data	Source	Content	Usage
DEM	Download from Geospatial Data Cloud	30 m spatial resolution	Sub-catchment division
Land use planning map	Norendar International LTD.	Impermeable rate, area, slope, etc.	Sub-catchment division
Pipe network data	Norendar International LTD.	Pipeline network slope, diameter, length, direction, etc.	Digitization of pipeline network
Precipitation	The Bureau of Hydrology and Water Resources Survey of Baoding	5 min/rainfall intensity monitored by Tilting rain gauge	Calibration and validation
Waterlogging data	Site survey	Waterlogging points, maximum waterlogging depth	Calibration and validation

Table A2. The calibration results of SWMM parameters.

Parameter Type	Parameter	Value Range	Value
Manning constant	N-imp	0.011~0.015	0.013
	N-perv	0.05~0.8	0.17
	Manning roughness coefficient	0~3	0.014
D-store	S-imp/mm	1.27~2.54	1.56
	S-prev/mm	2.54~7.62	3.5
Horton constant	Max-rate/(mm·h ⁻¹)	0~100	43
	Min-rate/(mm·h ⁻¹)	0~10	6
	Decay/(1·h ⁻¹)	0~7	3
	Dry time/d	1~7	7
the comprehensive runoff coefficient			0.692

Table A3. Parameters of LID layer.

LID Layer	Parameter	Permeable Pavements	Sunken Greenbelts	Rain Barrels
Surface layer	Berm Height/(mm)	2	200	-
	Vegetative Volume Fraction	0	0.85	-
	Surface Slope	1%	1%	-
	Surface Roughness	0.24	0.1	-
Pavement layer	Thickness/(mm)	150	-	-
	Void Ratio	0.15	-	-
	Impervious Surface Fraction	0	-	-
	Permeability/(mm/h)	200	-	-
	Clogging Factor	0	-	-
Soil layer	Thickness/(mm)	-	250	-
	Porosity	-	0.45	-
	Field Capacity	-	0.2	-
	Wilting Point	-	0.1	-
	Conductivity/(mm/h)	-	125	-
	Conductivity Slope	-	10	-
	Suction Head/(mm)	-	50	-

Table A3. Cont.

LID Layer	Parameter	Permeable Pavements	Sunken Greenbelts	Rain Barrels
Storage layer	Barrel Height/(mm)	300	300	1500
	Void Ratio	0.4	0.45	-
	Seepage Rate/(mm/h)	3.19	125	-
	Clogging Factor	0	-	-

References

- Raymond, C.; Horton, R.M.; Zscheischler, J.; Martius, O.; AghaKouchak, A.; Balch, J.; Bowen, S.G.; Camargo, S.J.; Hess, J.; Kornhuber, K.; et al. Understanding and managing connected extreme events. *Nat. Clim. Chang.* **2020**, *10*, 611–621. [\[CrossRef\]](#)
- Richard, P.; Allan, B.; Soden, J. Atmospheric warming and the amplification of precipitation extremes. *Science* **2008**, *321*, 1481–1484.
- Fischer, E.; Knutti, R. Anthropogenic contribution to global occurrence of heavy-precipitation and high-temperature extremes. *Nat. Clim. Chang.* **2015**, *5*, 560–564. [\[CrossRef\]](#)
- Guo, B.; Xie, T.; Zhang, W.; Wu, H.; Zhang, D.; Zhu, X.; Ma, X.; Wu, M.; Luo, P. Rasterizing CO₂ emissions and characterizing their trends via an enhanced population-light index at multiple scales in China during 2013–2019. *Sci. Total. Environ.* **2023**, *905*, 167309. [\[CrossRef\]](#)
- Wei, W.; Zou, S.; Duan, W.; Chen, Y.; Li, S.; Zhou, Y. Spatiotemporal variability in extreme precipitation and associated large-scale climate mechanisms in Central Asia from 1950 to 2019. *J. Hydrol.* **2023**, *620*, 129417. [\[CrossRef\]](#)
- Zhu, W.; Zha, X.; Luo, P.; Wang, S.; Cao, Z.; Lyu, J.; Zhou, M.; He, B.; Nover, D. A Quantitative Analysis of Research Trends in Flood Hazard Assessment. *Stoch. Environ. Res. Risk Assess.* **2023**, *37*, 413–428. [\[CrossRef\]](#)
- Zhang, G.; Mao, J.; Hua, W.; Wu, X.; Sun, R.; Yan, Z.; Liu, Y.; Wu, G. Synergistic effect of the planetary-scale disturbance, typhoon and Meso- β -scale convective vortex on the extremely intense rainstorm on 20 July 2021 in Zhengzhou. *Adv. Atmos. Sci.* **2023**, *40*, 428–446. [\[CrossRef\]](#)
- Wang, S.; Luo, P.; Xu, C.; Zhu, W.; Cao, Z.; Steven, L. Reconstruction of Historical Land Use and Urban Flood Simulation in Xi'an, Shannxi, China. *Remote Sens.* **2022**, *14*, 6067. [\[CrossRef\]](#)
- Luo, P.; Wang, X.; Zhang, L.; Zainol, M.; Duan, W.; Hu, M.; Guo, B.; Zhang, Y.; Wang, Y.; Daniel, N. Future Land Use and Flood Risk Assessment in the Guanzhong Plain, China: Scenario Analysis and the Impact of Climate Change. *Remote Sens.* **2023**, *15*, 5778. [\[CrossRef\]](#)
- Loperfido, J.V.; Gregory, B.; Noe, S.; Taylor, J.; Dianna, M.H. Effects of distributed and centralized stormwater best management practices and land cover on urban stream hydrology at the catchment scale. *J. Hydrol.* **2014**, *519*, 2584–2595. [\[CrossRef\]](#)
- Qi, W.; Ma, C.; Xu, H.; Chen, Z.; Zhao, K.; Han, H. Low Impact Development measures spatial arrangement for urban flood mitigation: An exploratory optimal framework based on source tracking. *Water Resour. Manag.* **2015**, *35*, 3755–3770. [\[CrossRef\]](#)
- Andersson, E.; Barthel, S.; Borgström, S.; Colding, J.; Elmqvist, T.; Folke, C.; Gren, Å. Reconnecting cities to the Biosphere: Stewardship of green infrastructure and urban ecosystem services. *AMBIO* **2014**, *43*, 445–453. [\[CrossRef\]](#) [\[PubMed\]](#)
- Cotterill, S.; Bracken, L.J. Assessing the effectiveness of Sustainable Drainage Systems (SuDS): Interventions, impacts and challenges. *Water* **2020**, *12*, 3160. [\[CrossRef\]](#)
- Wu, W.; Behzad, J.; Zhang, K.; Lucy, M.; Ana, D. Water Sensitive Urban Design (WSUD) Spatial Prioritisation through Global Sensitivity Analysis for effective urban pluvial flood mitigation. *Water Res.* **2023**, *235*, 119888. [\[CrossRef\]](#) [\[PubMed\]](#)
- Marjorie, R.V.R. Water sensitive residential developments: Application of LIUDD principles and methods in the Netherlands, Australia and New Zealand. *Urban Water J.* **2011**, *8*, 325–335.
- Chen, S.; Van de Ven, F.H.M.; Zevenbergen, C.; Verbeek, S.; Ye, Q.; Zhang, W.; Wei, L. Revisiting China's Sponge City Planning Approach: Lessons from a Case Study on Qinhuai District, Nanjing. *Environ. Sci.* **2021**, *9*, 748231. [\[CrossRef\]](#)
- Luo, P.; Yan, P.; Wang, X.; Wu, Y.; Lyu, J.; He, B.; Duan, W.; Wang, S.; Zha, X. Historical and Comparative Overview of Sponge Campus Construction and Future Challenges. *Sci. Total Environ.* **2024**, *907*, 167477. [\[CrossRef\]](#) [\[PubMed\]](#)
- Wang, B.; Chen, X.; Li, M.; Shen, Y.; Zhao, H. Discussion on the Reconstruction Design of Rainwater Pumping Station by Using Existing Underground Space for Regulation and Storage. *China Water Wastewater* **2019**, *35*, 64–67. [\[CrossRef\]](#)
- Kim, Y.; Han, M. Rainwater Storage Tank as a Remedy for a Local Urban Flood Control. *Water Sci. Tech. Water Supply* **2008**, *8*, 31–36. [\[CrossRef\]](#)
- Li, J.; Meng, G.; Che, W. On regulation, reservation and practical calculation in urban rainwater utilization. *WaterWastewater Eng.* **2007**, *33*, 42–46.
- Di Matteo, M.; Liang, R.; Maier, H.R.; Thyer, M.A.; Simpson, A.R.; Dandy, G.C.; Ernst, B. Controlling rainwater storage as a system: An opportunity to reduce urban flood peaks for rare, long duration storms. *Environ. Model. Softw.* **2019**, *111*, 34–41. [\[CrossRef\]](#)
- Chen, X.; Zhang, K.; Luo, Y.; Zhang, Q.; Zhou, J.; Fan, Y.; Huang, P.; Yao, C.; Chao, L.; Bao, H. A Distributed Hydrological Model for Semi-humid Watersheds with a Thick Unsaturated Zone Under Strong Anthropogenic Impacts: A Case Study in Haihe River Basin. *J. Hydrol.* **2023**, *623*, 129765. [\[CrossRef\]](#)

23. Wang, S.; Yi, B.; Wang, J.; Zheng, Q.; Gao, R.; Jing, M.; Qu, D. Infoworks simulation and plan design of urban rainwater storage pumping station. *China Water Wastewater* **2019**, *35*, 47–52. [[CrossRef](#)]
24. Baek, S.S.; Choi, D.H.; Jung, J.W.; Lee, H.J.; Lee, H.; Yoon, K.S.; Cho, K.H. Optimizing low impact development (LID) for stormwater runoff treatment in urban area, Korea: Experimental and modeling approach. *Water Res.* **2015**, *86*, 122–131. [[CrossRef](#)] [[PubMed](#)]
25. Kwak, D.; Kim, H.; Han, M.; Kim, J.H.; Kim, H.S.; Yoo, D.G.; Jung, D.; Song, C.G. Runoff control potential for design types of Low Impact Development in small developing area using XP SWMM. *Procedia Eng.* **2016**, *154*, 1324–1332. [[CrossRef](#)]
26. Kim, H.; Mallari, K.J.B.; Baek, J.; Pak, G.; Choi, H.I.; Yoon, J. Considering the effect of groundwater on bioretention using the Storm Water Management Model. *J. Environ. Manag.* **2019**, *231*, 1270–1276. [[CrossRef](#)] [[PubMed](#)]
27. Zhang, W.; Hou, J.; Shen, T.; Zhang, Y.; Li, D.; Wang, J.; Zhang, J. An optimal design method for low-impact development (LID) facilities based on the hydrodynamic model and genetic algorithm-assisted decision-making. *Water Policy* **2023**, *25*, 313–337. [[CrossRef](#)]
28. Chen, Y.; Tan, M.; Wan, J.; Weise, T.; Wu, Z. Effectiveness evaluation of the coupled LIDs from the watershed scale based on remote sensing image processing and SWMM simulation. *Eur. J. Remote Sens.* **2020**, *54*, 77–91. [[CrossRef](#)]
29. Tansar, H.; Duan, H.F.; Mark, O. Catchment-scale and local-scale based evaluation of LID effectiveness on urban drainage system performance. *Water Resour. Manag.* **2022**, *36*, 507–526. [[CrossRef](#)]
30. Chen, P.Y.; Tung, C.P.; Li, Y.H. Low Impact Development planning and adaptation decision-making under climate change for a community against pluvial flooding. *Water* **2017**, *9*, 756. [[CrossRef](#)]
31. Lee, J.; Kim, J.; Lee, J.M.; Jang, H.S.; Park, M.; Min, J.H.; Na, E.H. Analyzing the impacts of sewer type and spatial distribution of LID facilities on urban runoff and non-point source pollution using the Storm Water Management Model (SWMM). *Water* **2022**, *14*, 2776. [[CrossRef](#)]
32. Wang, Z.; Li, S.; Wu, X.; Lin, G.; Lai, C. Impact of spatial discretization resolution on the hydrological performance of layout optimization of LID practices. *J. Hydrol.* **2022**, *612*, 128113. [[CrossRef](#)]
33. Du, Y.; Hou, J.; Ma, H.; Liu, Q.; Wang, X.; Zhang, Z.; Chen, G. Spatial Pattern Optimization of LID Facility Based on SWMM. *China Water Wastewater* **2021**, *37*, 120–125.
34. Khoa Bui, X.; Marlim, M.S.; Kang, D. Water Network Partitioning into District Metered Areas: A State-of-the-Art Review. *Water* **2020**, *12*, 1002. [[CrossRef](#)]
35. Borzi, I. Evaluating Sustainability Improvement of Pressure Regime in Water Distribution Systems Due to Network Partitioning. *Water* **2022**, *14*, 1787. [[CrossRef](#)]
36. Di Nardo, A.; Di Natale, M.; Giudicianni, C.; Santonastaso, G.F.; Tzatchkov, V.; Varela, J.M.R.; Yamanaka, V.H.A. Water Supply Network Partitioning Based on Simultaneous Cost and Energy Optimization. *Procedia Eng.* **2016**, *162*, 238–245. [[CrossRef](#)]
37. Luan, Q.; Qin, Z.; Wang, D.; Liu, J.; Fu, X. Review on monitoring technology of urban road waterlogging after rainstorm and its application. *Water Resour. Prot.* **2022**, *38*, 106–116+140.
38. Liu, L.; Chen, M.; Luo, P.; Duan, W.; Hu, M.; Elbeltagi, A. A Novel Integrated Spatiotemporal-Variable Model of Landscape Changes in Traditional Villages in the Jinshaan Gorge, Yellow River Basin. *Land* **2023**, *12*, 1666. [[CrossRef](#)]
39. Wang, S.; Zhang, K.; Chao, L.; Chen, G.; Xia, Y.; Zhang, C. Investigating the feasibility of using satellite rainfall for the integrated prediction of flood and landslide hazards over Shaanxi Province in northwest China. *Remote Sens.* **2023**, *15*, 2457. [[CrossRef](#)]
40. Deng, H.; Pepin, N.C.; Chen, Y.; Guo, B.; Zhang, S.; Zhang, Y.; Chen, X.; Gao, L.; Liu, M.; Chen, Y. Dynamics of Diurnal Precipitation Differences and Their Spatial Variations in China. *J. Appl. Meteorol. Climatol.* **2022**, *61*, 1015–1027. [[CrossRef](#)]
41. Zhu, W.; Cao, Z.; Luo, P.; Tang, Z.; Zhang, Y.; Hu, M.; He, B. Urban Flood-Related Remote Sensing: Research Trends, Gaps and Opportunities. *Remote Sens.* **2022**, *14*, 5505. [[CrossRef](#)]
42. Liu, L.; Chen, M.; Luo, P.; Duan, W.; Hu, M. Quantitative Model Construction for Sustainable Security Patterns in Social–Ecological Links Using Remote Sensing and Machine Learning. *Remote Sens.* **2023**, *15*, 3837. [[CrossRef](#)]
43. Zhao, L.; Li, H.; Huang, W.; Dong, Y.; Geng, Y.; Ma, H.; Chen, J. Outbreak Mechanism of Locust Plagues under Dynamic Drought and Flood Environments Based on Time Series Remote Sensing Data: Implication for Identifying Potential High-Risk Locust Areas. *Remote Sens.* **2023**, *15*, 5206. [[CrossRef](#)]
44. Mei, C.; Liu, J.; Wang, H.; Li, Z.; Xia, L.; Wang, Y. Introduction of basic principle and application prospect for SWMM. *Water Resour. Hydropower Eng.* **2017**, *48*, 33–42.
45. Fu, X.; Wang, D.; Luan, Q.; Liu, J.; Wang, H. SWMM-based rainfall-runoff simulations in large-scale urban area with no pipeline-flow observations: II: Model calibration and analysis of rainfall-runoff simulations. *Adv. Water Sci.* **2020**, *31*, 51–60.
46. Su, X.; Yang, C.; Luan, Q.; Zhang, K.; Zhang, W. Simulation of flood control and storm drainage in typical northern urban district through MIKE URBAN. *J. Beijing Norm. Univ. (Nat. Sci.)* **2020**, *56*, 368–375. [[CrossRef](#)]
47. Xu, H.; Wang, Y.; Fu, X.; Wang, D.; Luan, Q. Urban flood modeling and risk assessment with limited observation data: The Beijing future science city of China. *Int. J. Environ. Res. Public Health* **2023**, *20*, 4640. [[CrossRef](#)] [[PubMed](#)]
48. Lewis, A.R. *Storm Water Management Model User’s Manual Version 5.1*; The United States Environmental Protection Agency (USEPA): Washington, DC, USA, 2015.
49. Lu, X.; Chan, F.K.S.; Li, N.; Chen, C.K.; Chen, W.Q.; Chan, H.K. Improving urban flood resilience via GDELT GKG analyses in China’s Sponge Cities. *Sci. Rep.* **2022**, *12*, 20317. [[CrossRef](#)]

50. Abdul Jaleel, Y.; Demissie, Y. Identifying cost-effective Low-Impact Development (LID) under climate change: A multi-objective optimization approach. *Water* **2022**, *14*, 3017. [[CrossRef](#)]
51. Huo, Y. *Study on the Effectiveness of Runoff Reducing and Control through Concave Greenbelt Measures*; Hebei University of Engineering: Handan, China, 2019.
52. Wei, Y. *Study on Risk Assessment of Urban Rainwater Pipelines and Optimized Operation of Rainwater Pump Station*; Hefei University of Technology: Hefei, China, 2019.
53. Peng, J.; Yu, L.; Zhong, X.; Dong, T. Study on runoff control effect of different drainage schemes in sponge airport. *Water Resour. Manag.* **2022**, *36*, 1043–1055. [[CrossRef](#)]
54. Wu, Y.; She, D.; Xia, J.; Song, J.; Xiao, T.; Zhou, Y. The quantitative assessment of impact of pumping capacity and LID on urban flood susceptibility based on machine learning. *J. Hydrol.* **2023**, *617*, 129116. [[CrossRef](#)]

Disclaimer/Publisher’s Note: The statements, opinions and data contained in all publications are solely those of the individual author(s) and contributor(s) and not of MDPI and/or the editor(s). MDPI and/or the editor(s) disclaim responsibility for any injury to people or property resulting from any ideas, methods, instructions or products referred to in the content.